ACS APPLIED MATERIALS & INTERFACES

Research Article

www.acsami.org

Drug/Dye-Loaded, Multifunctional PEG–Chitosan–Iron Oxide Nanocomposites for Methotraxate Synergistically Self-Targeted Cancer Therapy and Dual Model Imaging

Jinyan Lin,[†] Yang Li,[†] Yanxiu Li,[†] Hongjie Wu,[§] Fei Yu,[#] Shuifan Zhou,[†] Liya Xie,[⊥] Fanghong Luo,[∥] Changjian Lin,[†,‡] and Zhenqing Hou*[,†,◊,♦]

[†]Department of Biomaterials and Department of Materials Science and Engineering and [♦]Research Center of Biomedical Engineering and Institute of Soft Matter and Biomimetics, College of Materials, Xiamen University, Xiamen 361005, China

[‡]Department of Chemistry and [#]Department of Chemical and Biochemical Engineering, College of Chemistry and Chemical Engineering, Xiamen University, Xiamen 361005, China

[§]Department of Pharmacy, School of Pharmaceutical Science, Xiamen University, Xiamen 361102, China

[∥]Cancer Research Center, Medical College, Xiamen University, Xiamen 361005, China

[⊥]The First Affiliated Hospital of Xiamen University, Xiamen 361002, China

[◊]Department of Physics, Changji University, Changji 831100, China

ABSTRACT: Multifunctional nanocomposites hold great potential to integrate therapeutic and diagnostic functions into a single nanoscale structure. In this paper, we prepared the MTX-PEG-CS-IONPs-Cy5.5 nanocomposites by functionalizing the surface of chitosan-decorated iron oxide nanoparticles (CS-IONPs) with polyethylene glycolated methotraxate (MTX-PEG) and near-infrared fluorescent cyanin dye (Cy5.5). A clinically useful PEGylated anticancer prodrug, MTX-PEG, was also developed as a tumor cell-specific targeting ligand for self-targeted cancer treatment. In such nanocomposites, the advantage was that the orthogonally functionalized, self-targeted MTX-PEG-CS-IONPs-Cy5.5 can synergistically combine an early phase selective tumor-targeting efficacy with a late-phase cancer-killing effect, which was also confirmed by dual model (magnetic resonance and fluorescence) imaging. Furthermore, with the aids of the folate (FA) receptor-mediated endocytosis (able to turn cellular uptake "off" in normal cells and "on" in cancer cells) and pH/intracellular protease-mediated hydrolyzing peptide bonds (able to turn drug release "off" in systemic circulation and "on" inside endo/lysosomes), the MTX-PEG-CS-IONPs-Cy5.5 could deliver MTX to FA receptors-overexpressed cancer cells, showing the improved anticancer activity with the reduced side effects. Together, the MTX-PEG-CS-IONPs-Cy5.5 could act as a highly convergent, flexible, and simplified system for dual model imaging and synergistically self-targeted cancer therapy, holding great promise for versatile biomedical applications in future.

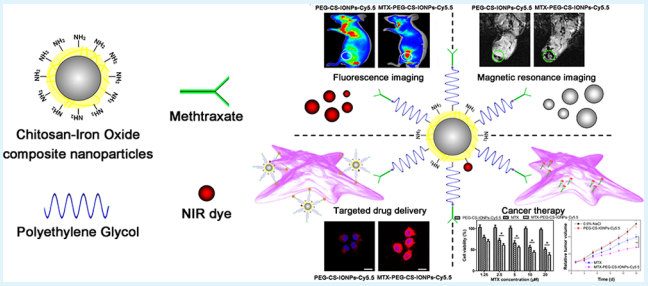

KEYWORDS: *MTX-PEG, magnetic resonance imaging, drug delivery, self-targeted cancer therapy*

1. INTRODUCTION

Nanoparticles (NPs) represent a potent tool in the field of biomedicine for targeting drug delivery and imaging of cancer,[1] which is a major public problem worldwide.[2] In particular, some types of NPs have attracted intense attention in cancer imaging, diagnostics, and therapy due to their unique size-dependent electronic, optical, and magnetic properties.[3] For instance, magnetic NPs have been utilized for targeted drug delivery,[4] magnetic resonance imaging,[4−6] and hyperthermia therapy.[7] Semiconductor NPs have been used as fluorescent probes for cell tracking, imaging, and diagnostics.[8,9] Noble metal NPs have been used in imaging, sensing, targeted drug delivery, and photothermal therapy.[10] However, the development of the multifunctional NPs that have structural and functional advantages compared with bulk material and single molecules is a burgeoning research area.[4] In this regard, as compared with the NPs with a single function, the multifunctional NPs offered great opportunities to meet the increasing demands in potential biomedical applications such as imaging, diagnostics, and therapy.[11]

Although superparamagnetic iron oxide NPs (IONPs) have recently attracted considerable attention in cancer therapy and diagnosis, the poor physiological stability, rapid blood clearance from the circulation, and, especially, the lack of target specificity of the IONPs as drug delivery systems limited their availability for clinical use.[12−16] However, the integration of multiple

Received: February 23, 2015
Accepted: May 15, 2015
Published: May 15, 2015

DOI: 10.1021/acsami.5b01685
ACS Appl. Mater. Interfaces 2015, 7, 11908−11920

functions into the IONPs to develop the systemically administrated and cancer-specific drug delivery systems was a formidable challenge, since adding new functionality inevitably elevates complexity (such as multistep synthesis, purification, and characterization) and cost and lowers controllability (such as multicomponent and heterogeneous formulations).[17] More importantly, achieving the flexible and reasonable combination of targeted drug delivery and cancer therapy of the IONPs drug delivery systems as well as reducing their structural complexity was still highly desirable for clinical application. As is well-known, the IONPs have no specific functional groups on the surface, which restricted the further biomedical applications. Our group previously reported that biocompatible and biodegradable chitosan (CS) was assembled on the surface of the IONPs using a nonsolvent-aided coacervation procedure and a chemical cross-linking procedure,[18,19] which could not only improve the colloidal stability of the IONPs but also facilitate the surface biomodification of the IONPs.[18−20] The in vitro and in vivo results further inspired our motivation of using the CS-IONPs as drug vehicles to continue our studies for imaging, diagnostics, and targeted cancer therapy.

In this paper, polyethylene glycol (PEG), well-known to reduce nonspecific adsorption of plasma proteins, was used to make these NPs biocompatible and be well-dispersed in aqueous environment. Methotrexate (MTX), a potent antimetabolite and anticancer drug that suppressed the activity of dihydrofolate reductase (DHFR) enzyme and interrupt the folate (FA) cycle for the inhibition of nucleic acid biosynthesis and cell proliferation,[21,22] was introduced to these NPs as drug delivery carriers for cancer therapy. It was well-known that the functionalization of tumor-targeting agents on the NP surface is another strategy to enhance the tumor accumulation and improve the drug efficacy. Antibody, peptides, proteins, aptamers, vitamins, and polysaccharides have been developed as active targeting ligands.[23] However, MTX as an anticancer drug could also be exploited as a tumor-specific targeting ligand to self-direct these NPs to cancer cells overexpressing folate (FA) receptor by virtue of high structural similarity between MTX and FA[20,24−27] (MTX and FA could be uptaken into cells by reduced FA carrier,[28] proton-coupled FA transporter,[29] and membrane-associated FA receptor[28,30]). In particular, the dual role of MTX has recently drawn attention, which might open exciting new opportunities.[31−33] In addition, to satisfy the need for the potentially rapid clinical development of highly convergent, flexible, and simplified targeted cancer therapy, it was necessary to introduce the fluorescence imaging capability into these NP-based drug delivery systems to enable the noninvasive assessment of drug delivery.

Herein, we report a facile strategy to synthesize the NPs with cancer cell self-targeting/kill ability, fluorescence character, and superparamagnetic property for simultaneous cancer diagnosis and therapy. The IONPs were fabricated by a chemical coprecipitation method first.[34] And then CS-IONPs were prepared by a nonsolvent-aided coacervation procedure followed by a chemical cross-linking procedure.[19,20] After that, PEGylated MTX prodrug (MTX-PEG) and Cy5.5 dye were functionalized on the surface of the CS-IONPs via carbodiimide chemistry. Our synthesized NPs had four key components. First, the IONPs were selected as a superparamagnetic core for magnetic resonance imaging. Second, CS was employed for the IONPs coating to introduce additional properties that were desirable for biofunctionlization. Third, near-infrared (NIR) dye Cy5.5 exhibited the intense NIR emission, which was ideal for deep-tissue fluorescence imaging. Fourth, MTX was used not only as a tumor-specific targeting ligand at an early phase for targeting but also as a enzyme-specific anticancer drug at a late phase for anticancer. The evaluations of both in vitro and in vivo functions of the multifunctional and therapeutic NPs for multimodal (fluorescence and magnetic resonance) imaging cooperated with self-targeted cancer therapy have not been studied before.

2. EXPERIMENTAL SECTION

2.1. Materials. All chemicals were of reagent grade and used without further purification. Iron(III) chloride hexahydrate ($FeCl_3·6H_2O$, 99%), iron(II) sulfate heptahydrate ($FeSO_4·7H_2O$, 99%) glutaraldehyde solution (25%), and sodium borohydride were purchased from West Long Chemical Co., Ltd. Chitosan (CS, MW = 5000 Da, 95% degree of deacetylation) was purchased from Zhejiang Aoxing Biotechnology Co., Ltd. (Zhengjiang, China). 1-(3-(Dimethylamino)propyl)-3-ethylcarbodiimide (EDC), *N*,*N*′-dicyclohexylcarbodiimide (DCC), *N*-hydroxysuccinimide (NHS), protease type I: crude protease from bovine pancreas, and Hoechst 33258 were obtained from Sigma-Aldrich (St. Louis, MO). Bifunctional PEG (NH_2−PEG−COOH, MW = 5000 Da) was purchased from Beijing Kaizheng Biotech Development Co., Ltd. (Beijing, China). mPEG-SPA (MW = 5000 Da) was from Jiaxing Biomatrik (China). Methotrexate (MTX) and folate (FA) were purchased from Bio Basic Inc. (Markham, Ontario, Canada). Cy5.5 NHS ester was purchased from GE Healthcare, formerly Amersham Biosciences (Amersham, U.K.). Water was deionized (DI) and filtered with 0.22 mm polycarbonate membranes. Fetal bovine serum (FBS) was from Gibco Life Technologies (AG, Switzerland). Trypsin (0.25%), ethylenediaminetetraacetic acid, and penicillin−streptomycin solution were from Invitrogen. Dulbecco's Modified Eagle's Medium (DMEM) was from Sigma Chemical Corp.

2.2. Synthesis of MTX-PEG. MTX-PEG was synthesized using a two-step procedure via carbodiimide chemistry between MTX and bifunctional PEG. The first step was to prepare the activated MTX NHS ester using DCC/NHS. Briefly, MTX (0.320 g, 0.705 mmol) was activated by 0.174 g of DCC (0.846 mmol) and 0.097 g of NHS (0.846 mmol) in anhydrous dimethylformamide (DMF) for 18 h. Thin-layer chromatography (TLC) analysis was performed to ensure the completion of reaction. Subsequently, the reaction mixture was filtered to remove the precipitated DCU, and the filtrate was precipitated in ice-cold ether. The crude precipitate was further washed by dichloromethane (DCM) to remove the excess, unreacted starting material, and then dried under vacuum overnight. The second step was to prepare the MTX-PEG between the activated MTX NHS ester and bifunctional PEG. Briefly, MTX-NHS ester (0.200 g, 0.363 mmol) was dissolved in DMF containing triethylamine (TEA; 0.726 mmol). Then, NH_2−PEG−COOH (1.210 g, 0.242 mmol) dissolved in DMF was carefully added dropwise to the resultant solution. The reaction mixture was vigorously stirred under a nitrogen atmosphere for 24 h at 0 °C. TLC analysis was performed to ensure the completion of reaction. The reaction mixture was filtered, precipitated in ice-cold ether, and collected by centrifugation at 6000 rpm for 20 min at 4 °C. The yellow precipitate was dissolved in DCM and then centrifugated at 6000 rpm for 20 min. The supernatant was filtered, rotary evaporated, and dried under vacuum overnight. The product redissolved in DI water was highly purified by dialysis (Mw = 6000 Da) against DI water for 72 h, filtration with 0.22 mm polycarbonate membranes, and lyophilization for 48 h. ^{1}H NMR spectrum was recorded with a Bruker AV400 MHz NMR spectrometer (Billerica, MA). UV−vis spectrum was analyzed using a UV−vis spectrometer (DU800 Beckman Coulter, Brea, CA).

2.3. Preparation of MTX-PEG-CS-IONPs-Cy5.5. Initially, the IONPs were fabricated by a classic chemical coprecipitation[12,34] with minor modification of 4.73 g of $FeCl_3·6H_2O$ and 2.78 g of $FeSO_4·7H_2O$ in 100 mL of DI water with addition of NH_4OH.[18] Second, the CS-IONPs were prepared using the prepared IONPs and CS by a nonsolvent-aided coacervation procedure[18] followed by a chemical cross-linking procedure as we have reported previously.[20,22] Third, the MTX-PEG-CS-IONPs were prepared by conjugating the carboxy group of MTX-PEG to the amine group of CS-IONPs using carbodiimide

DOI: 10.1021/acsami.5b01685
ACS Appl. Mater. Interfaces 2015, 7, 11908−11920

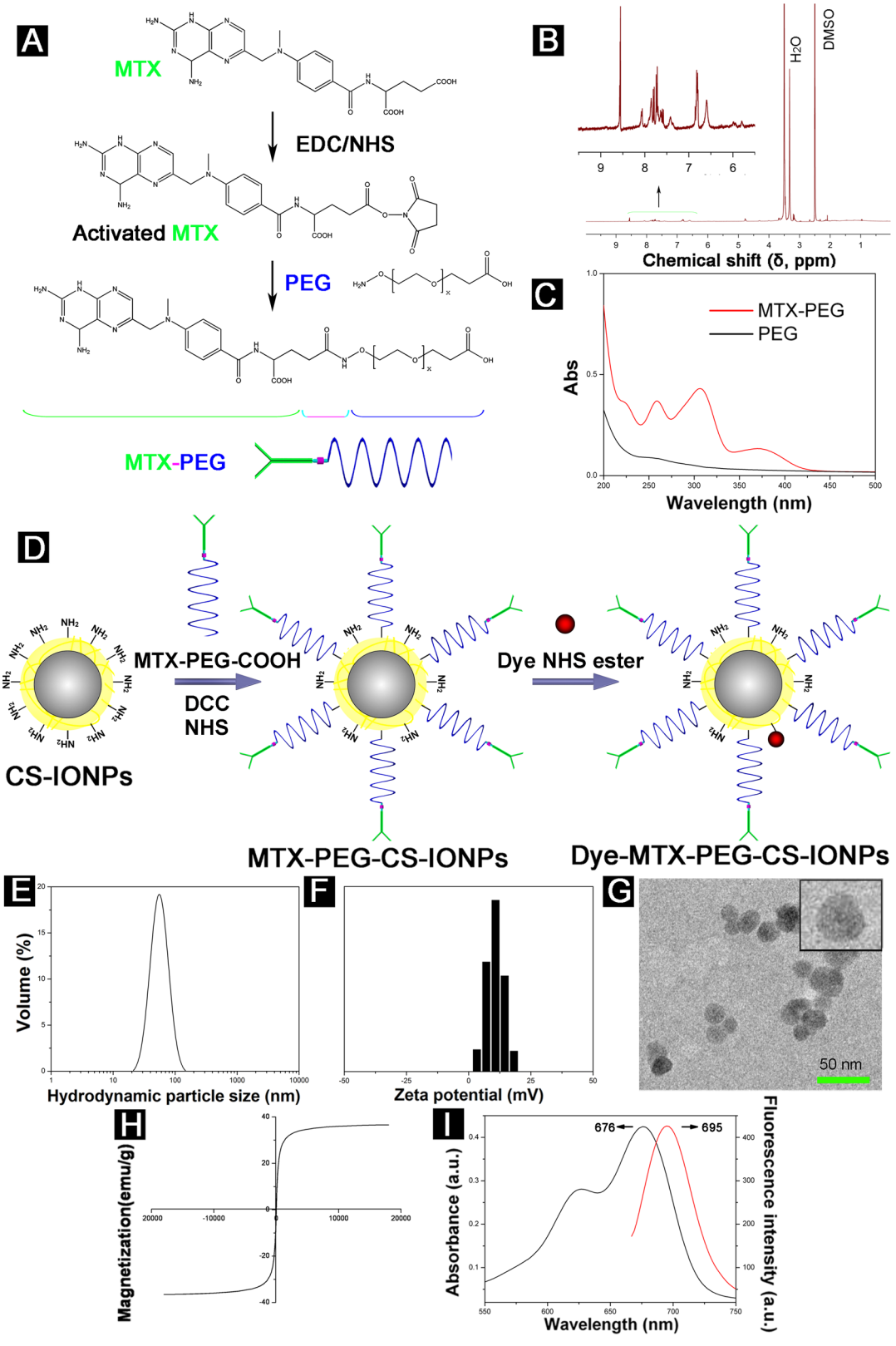

Figure 1. (A) Synthetic routes of MTX-PEG. (B) ^{1}H NMR spectrum of MTX-PEG. (C) UV−vis spectrum of MTX-PEG. (D) Schematic illustration of the synthetic procedure for the MTX-PEG-CS-IONPs-Cy5.5. (E) Hydrodynamic particle size and particle size distribution of the MTX-PEG-CS-IONPs-Cy5.5. (F) Zeta potential of the MTX-PEG-CS-IONPs-Cy5.5. (G) TEM image of the MTX-PEG-CS-IONPs-Cy5.5. (inset) Enlarged image. (H) Magnetization curve of the MTX-PEG-CS-IONPs-Cy5.5. (I) UV−vis absorption and fluorescence spectrum of the MTX-PEG-CS-IONPs-Cy5.5.

chemistry. In brief, MTX-PEG (0.918 g, 0.169 mmol), 0.039 g of EDC (0.202 mmol), and 0.023 g of NHS (0.202 mmol) were added to the CS-IONPs suspension (pH 7.4) accompanied by vigorous stirring under nitrogen atmosphere for 8 h in the dark. The resultant MTX-PEG-CS-IONPs were centrifugated at 12 000 rpm for 15 min and washed with DI water thrice. The precipitates were redispersed in DI water, dialyzed

DOI: 10.1021/acsami.5b01685
ACS Appl. Mater. Interfaces 2015, 7, 11908−11920

(Mw = 8000 to 14 000 Da) against DI water for 48 h, and lyophilized for 24 h. For fluorescence imaging, the MTX-PEG-CS-IONPs were labeled with Cy5.5 (mass ratio of Cy5.5 and MTX-PEG-CS-IONPs = 0.05) between the residual amine groups and the *N*-hydroxysuccinimide activated ester groups.[6] In addition, the PEG-CS-IONPs-Cy5.5 were prepared using the same method with MTX-PEG replaced by mPEG-SPA at the same mass and used for comparison.

2.4. Characterization of MTX-PEG-CS-IONPs-Cy5.5. The hydrodynamic particle size, polydispersity index (PDI), and zeta potential of the MTX-PEG-CS-IONPs-Cy5.5 were evaluated by a Malvern Zetasizer Nano-ZS (Malvern Instruments, Worcestershire, U.K.). The morphology of the MTX-PEG-CS-IONPs-Cy5.5 was visualized by transmission electron microscope (TEM, JEM 1400, JEOL, Tokyo, Japan). The superparamagnetic properties of the MTX-PEG-CS-IONPs-Cy5.5 were measured by a vibrating sample magnetometer (VSM-7400, Lakeshore). The UV−vis absorption spectrum of the MTX-PEG-CS-IONPs-Cy5.5 was performed on a Beckman Coutler DU-800 UV−vis spectrometer. The fluorescence spectrum of the MTX-PEG-CS-IONPs-Cy5.5 was collected by a FLS920 Fluorescence Lifetime and Steady State Spectrometer.

2.5. Drug-Loading Content. The drug amount was determined by a high-performance liquid chromatography (HPLC, Waters Associates, Milford, MA) system using a Hypersil ODS column (250 mm × 4.6 mm, 5 μm). The mobile phase flow rate was 1.0 mL/min. The mobile phase was HPLC grade 40 mM potassium dihydrogen phosphate (pH 4.5)/acetonitrile (88/12, v/v). The detection wavelength was 303 nm. The drug-loading content was calculated by the formula as previously reported.[35]

2.6. In Vitro Physiological Stability. The MTX-PEG-CS-IONPs-Cy5.5 were suspended in H_2O, PBS, 0.9% (w/v) NaCl, 10% (v/v) plasma/heparin in PBS, RPMI 1640, or fetal bovine serum (FBS) at 37 °C over 24 h of incubation. The particle size stability test of the MTX-PEG-CS-IONPs-Cy5.5 was assayed at different time points by dynamic light scattering (DLS). The fluorescence stability test of the MTX-PEG-CS-IONPs-Cy5.5 suspensions was also assayed at different time points by a fluorescence spectrometer (F900, Edinburgh Instruments Ltd., U.K.). The PEG-CS-IONPs-Cy5.5 and CS-IONPs-Cy5.5 were used for comparison.

2.7. In Vitro Drug Release. To simulate the extracellular conditions and intracellular lysosomal conditions, the MTX-PEG-CS-IONPs-Cy5.5 were suspended in 5 mL of PBS buffer solution (pH 5.0 or 7.4) with or without the crude protease from bovine pancreas and transferred to the dialysis bag. The dialysis was immersed in PBS at 37 °C and shaken at a speed of 100 rpm. At desired time intervals, 2 mL of the release media was withdrawn to determine the concentration of drug released from the NPs, and equal volume of fresh PBS was replenished. The free MTX was used for comparison.

2.8. Cell Culture. Human cervical carcinoma HeLa cells were provided by American Type Culture Collection (ATCC). HeLa cells were cultured in DMEM supplemented with 10% FBS and 1% penicillin−streptomycin. Since DMEM medium contained the free FA that suppressed the cell uptake mediated by the FA receptor of cancer cells, we used the FA-deficient culture medium: FA-deficient DMEM in the cellular experiments. The cells were cultivated in an incubator (Thermo Scientific) at 37 °C and 5% CO_2.

2.9. In Vitro Cellular Uptake. The qualitative cellular uptake of the MTX-PEG-CS-IONPs-Cy5.5 and PEG-CS-IONPs-Cy5.5 was observed by confocal laser scanning microscopy (Leica Microsystems, Mannheim, Germany) similar to a previously reported method.[20]

2.10. Flow Cytometry. The quantitative cellular uptake of the MTX-PEG-CS-IONPs-Cy5.5 and PEG-CS-IONPs-Cy5.5 was accomplished using flow cytometry similar to a previously reported method.[36]

2.11. In Vitro Cell Viability. The cell viability of the MTX-PEG-CS-IONPs-Cy5.5 was assayed using a MTT assay according to a previously reported method.[37] HeLa cells were treated with the MTX-PEG-CS-IONPs-Cy5.5, free MTX, and PEG-CS-IONPs-Cy5.5 with different MTX concentrations for 48 h.

2.12. Animals and Tumor Models. All animal procedures were in accordance with the guidelines of the institutional animal care and use committee at the Xiamen University. Adult Sprague−Dawley rats (200 ± 20 g) and BALB/C nude mice aged six weeks were provided from Shanghai Laboratory Animal Center, Chinese Academy of Sciences. The tumor model was established by subcutaneously inoculation of 1×10^6 HeLa cells in the selected positions of BALB/C nude mice. The tumor volume was calculated according to a previously reported method.[37]

2.13. In Vivo Pharmacokinetics. MTX-PEG-CS-IONPs-Cy5.5 (200 μL, 4 mg/kg) was injected intravenously via the tail vein of rats. At desired timed intervals, 200 μL of blood was collected in a heparinized tube and centrifuged at 3000 rpm to harvest the plasma. MTX were extracted from the plasma using 7% perchloric acid, centrifuged at 10 000 rpm for 10 min, and determined by a HPLC method as described above. The pharmacokinetic parameters were calculated by fitting the blood drug pharmaceutical concentrations to a two-compartment model using WinNonlin Professional Edition Version 2.1 (Pharsight Corporation, CA). The free MTX at the equivalent MTX concentration was used for comparison.

2.14. In Vivo Fluorescence Imaging. MTX-PEG-CS-IONPs-Cy5.5 (0.2 mL) or PEG-CS-IONPs-Cy5.5 (4 mg/kg) was injected into mice bearing HeLa tumor through the tail vein. In vivo fluorescence imaging was performed at different time points postinjection using a MaestroTM in vivo imaging system (Cambridge Research & Instrumentation, Woburn, MA). At 12 h postinjection, the mice were sacrificed. The tumor and normal tissues (heart, lung, kidney, spleen, and liver) were excised and washed with 0.9% NaCl for the ex vivo fluorescence imaging. The data were used to identify, separate, and remove the contribution of auto fluorescence in analyzed images.

2.15. In Vivo Magnetic Resonance Imaging. For magnetic resonance imaging, HeLa tumor-bearing mice were used as model. We performed the experiments of magnetic resonance imaging according to a method previously reported.[38] Briefly, the images were taken prior to the intravenous administration of and MTX-PEG-CS-IONPs-Cy5.5 (4 mg/kg) and at an appropriate time point postinjection. Mice received general drug anesthesia. Magnetic resonance imaging was performed using a 7 T MRI scanner (Varian 7 T Micro MRI System) with a fast gradient-echo sequence: TR = 100 ms; TE = 9 ms; slices = 5; slice thickness = 1 mm; averages = 2; field of view (Fov) read = 50 mm; matrix = 256 × 256; flip angle = 20 °C. The signal intensity of tumor regions of interest (ROI) in the tumor was then measured. The PEG-CS-IONPs-Cy5.5 were used for comparison.

2.16. In Vivo Anticancer Effect. HeLa tumor bearing mice were used as model of in vivo cancer therapy. The tumors were established in the mice by by subcutaneous inoculation of HeLa cells in the selected position of mice as described above. When tumors were ∼50−100 mm^3 in tumor size (volume), the mice were randomly divided into four groups. Every group included six mice. 0.9% NaCl, free MTX, PEG-CS-IONPs-Cy5.5, and MTX-PEG-CS-IONPs-Cy5.5 (4 mg/kg) were injected in four groups of HeLa tumor-bearing mice via the tail vein. Four groups were given three intravenous injections of drugs on days 1, 4, and 7, with the day of the first intravenous injection counted as day 1. Each mouse was earmarked and followed individually throughout the whole experiment. The tumor volume and body weight were then dertemined according to the method as described above every 2 d for two weeks until the euthanasia.

3. RESULTS AND DISCUSSION

3.1. Synthesis of MTX-PEG. The synthesis of MTX-PEG was illustrated in Figure 1. MTX−PEG was synthesized through the amide bond between the carboxyl end groups of MTX and the amine end groups of NH_2−PEG-COOH using DCC/NHS referring to the methods reported by Yoo et al. and Cao et al. with minor modification.[6,39] In a one-pot procedure (MTX, NH_2−PEG-COOH, DCC, and NHS were reacted together), the self-conjugation side product may exist. To minimize the occurrence of side reaction as far as possible, we proposed a two-step procedure under vigorous stirring on ice, using slightly excess DCC/NHS (1.2 equiv to MTX) and carefully controlling the sequence and speed of the feed.[39] In this procedure, MTX was activated using DCC/NHS first, and then the activated MTX was

DOI: 10.1021/acsami.5b01685
ACS Appl. Mater. Interfaces 2015, 7, 11908−11920

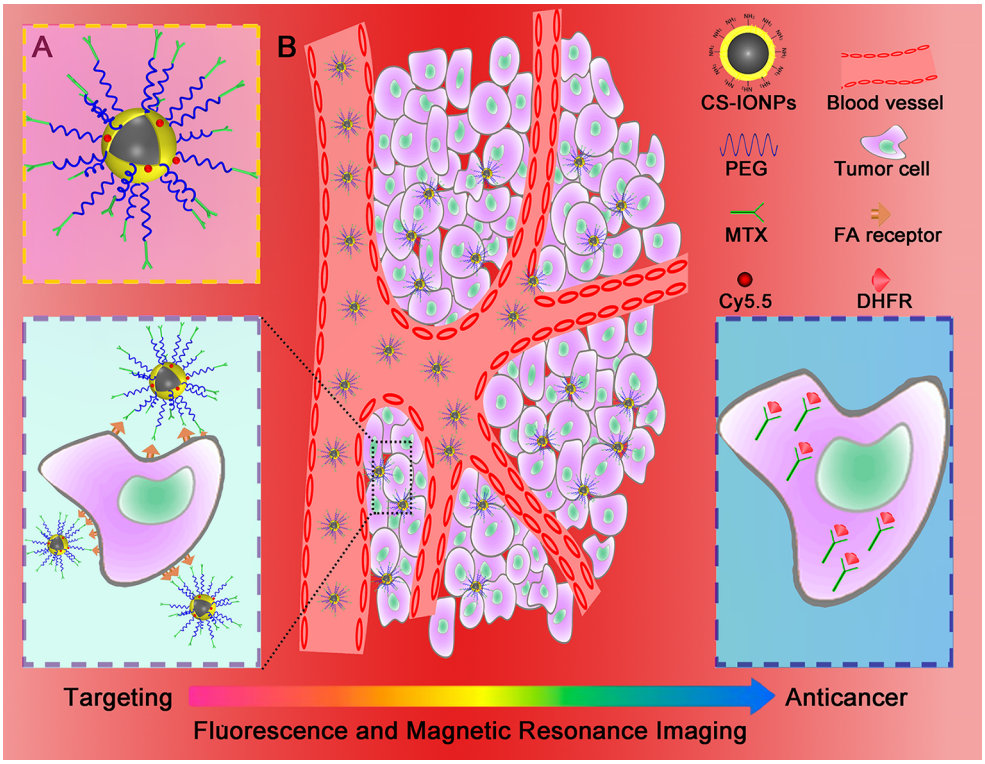

Figure 2. (A) Design of the multifunctional MTX-PEG-CS-IONPs-Cy5.5. (B) Schematic diagram of the MTX- PEG-CS-IONPs-Cy5.5s as the multifunctional system for targeted drug delivery and cancer therapy, enabling multimodel (fluorescence and magnetic resonance) imaging of tumor. The MTX-PEG-CS-IONPs comprised a magnetic IO core for magnetic resonance imaging, a CS layer for biofunctionalization, and a PEG shell for prolonged blood circulation. In addition, MTX was exploited as a tumor-targeting ligand and an anticancer drug, and Cy5.5 was used for fluorescence imaging. Once intravenously administrated, the MTX-PEG-CS- IONPs-Cy5.5 were accumulated at the tumor site via the enhanced permeability and retention (EPR) effect. And then the MTX-PEG-CS-IONPs-Cy5.5 were internalized by the tumor cells via FA receptor-mediated endocytosis. Lastly, the MTX-PEG-CS-IONPs-Cy5.5 released MTX via pH/intracellular proteases-mediated hydrolyzing peptide bonds and exposed the anticancer effect by the interaction of dihydrofolate reductase (DHFR) with MTX.

reacted with one terminal amine of biofunctional PEG. TLC analysis was performed to ensure the completion of reaction. The reaction mixture was precipitated, followed by dialyzation using DI water for a very long period of time, and was eventually lyophilized. As shown in ^{1}H NMR spectrum of MTX-PEG (Figure 1B), the characteristic peak at 3.5 ppm was assigned to the methylene protons of PEG units, and the characteristic peaks at 6.8, 7.7, and 8.6 ppm were attributed to the protons of the pteridine ring and *p*-phenyl ring of MTX.[26] In addition, the composition of MTX in MTX−PEG was measured by ^{1}H NMR analysis. The substitution value for MTX in PEGyalted MTX was ~97.8 mol % by calculating the integral ratio between the protons of PEG (at 3.5 ppm) and the protons of the *p*-phenyl ring in MTX (at 8.6 ppm). As shown in UV−vis spectrum of MTX-PEG (Figure 1C), the characteristic peaks at 259 and 306 nm were originated from the structure of MTX.[40] All of the results confirmed the successful conjugation between MTX drug and PEG macromolecule.

3.2. Preparation of MTX-PEG-CS-IONPs-Cy5.5. The preparation of the MTX-PEG-CS-IONPs-Cy5.5 and their combined application were, respectively, illustrated in Figures 1D and 2. The MTX-PEG molecules were used to be functionalized on the surface of the CS-IONPs between the carboxyl end groups of MTX-PEG molecules and the residual amine groups of the CS-IONPs via EDC-mediated coupling reaction. The designed MTX-PEG-CS-IONPs were prepared with a core-layer-shell structure. The IONP core was used for magnetic resonance imaging. The CS layer was rich of functional amino groups, which was facilitated the easy surface functionalization with a wide range of biomolecules. The CS layer, biocompatible and biodegradable polymer, could also serve as an effective physical barrier to lessen the contact between the IONPs and the dye to avoid the quenching of fluorescence.[41] PEG shell was used to make the NPs biocompatible and well-dispersible in aqueous media. More importantly, MTX was exploited as not only an early phase tumor cell-selective ligand but also a late-phase therapeutic anticancer drug, not only to facilitate the cellular uptake but also to induce the cell death. In addition, for in vitro and in vivo fluorescence imaging, we labeled the MTX-PEG-CS-IONPs with the NIR dye Cy5.5 via the amide linkage between the activated ester groups of NIR dye and the residual amine groups of the MTX-PEG-CS-IONPs.

3.3. Characterization of MTX-PEG-CS-IONPs-Cy5.5. In the fabrication of the MTX-PEG-CS-IONPs, the resultant product was highly purified by centrifugation, washing, and dialysis to remove the unreacted MTX-PEG, other starting materials (such as EDC and NHS), and various impurities. The preparation of the MTX−PEG−CS−IONPs was confirmed by the spectrum of Fourier transform infrared spectroscopy (FTIR, Thermo Scientific, UT; Figure 3A). The characteristic peaks at 596, 1113, 1558, 1650, 1714, 2877, and 3430 cm^{-1} were assigned to the Fe−O stretching vibration of the IONPs, C−O−C stretching vibration of PEG, C═O stretching vibration of amide II, C═O stretching vibration of amide I, C═O stretching vibration of MTX, alkyl C−H stretching vibration of PEG, and the overlap of N−H and O−H stretching vibration of CS,

DOI: 10.1021/acsami.5b01685
ACS Appl. Mater. Interfaces 2015, 7, 11908−11920

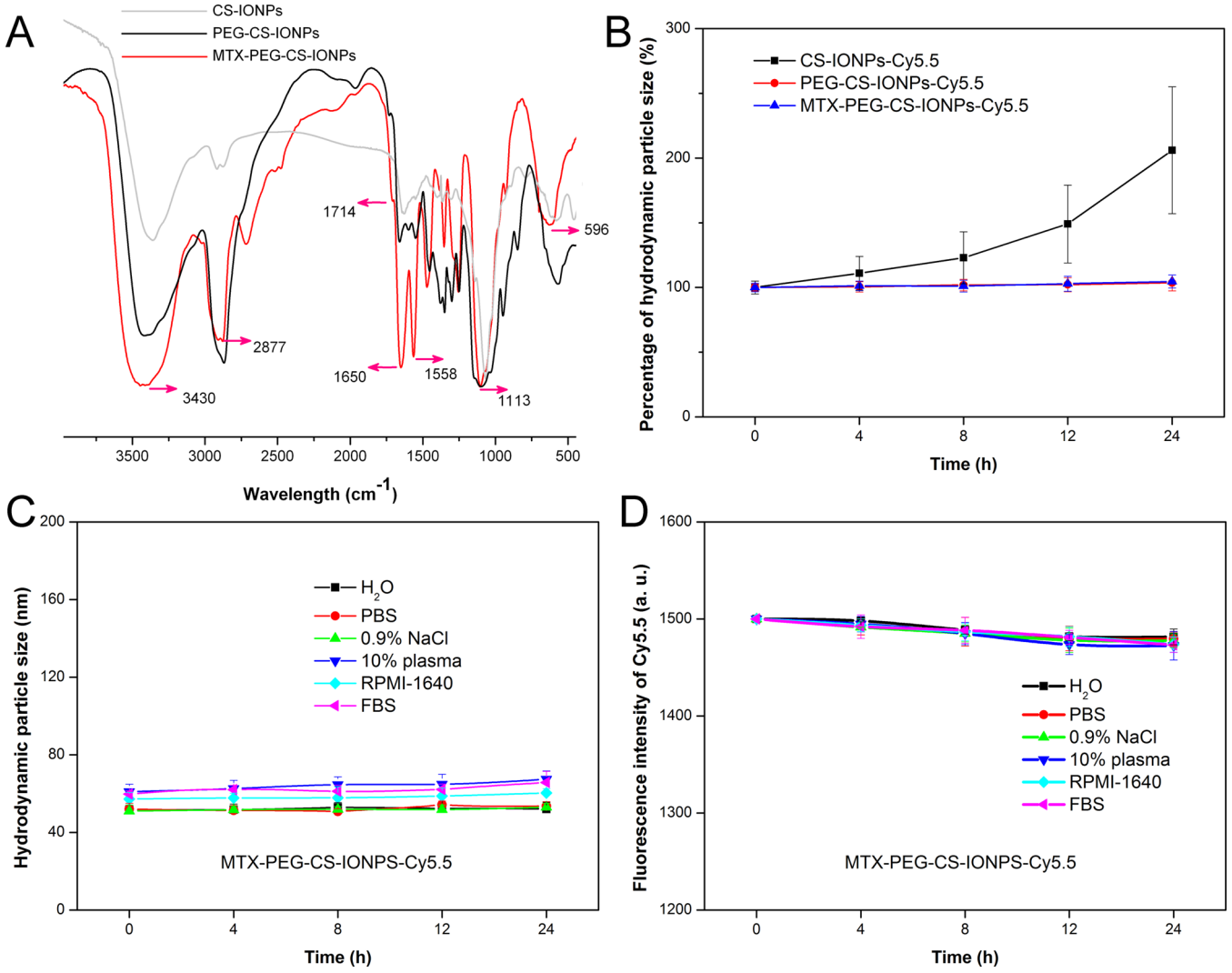

Figure 3. (A) FTIR spectra of the CS-IONPs, PEG-CS-IONPs, and MTX-PEG-CS-IONPs. (B) In vitro partile size stability of the CS-IONPs-Cy5.5, PEG-CS-IONPs-Cy5.5, and MTX-PEG-CS-IONPs-Cy5.5 in H_2O at 37 °C. Data were presented as mean ± standard deviation (SD; $n = 3$). (C) In vitro particle size stability of the MTX-PEG-CS-IONPs-Cy5.5 in H_2O, PBS, 0.9% NaCl, 10% plasma, RPMI 1640, and FBS at 37 °C. Data were presented as mean ± SD ($n = 3$). (D) Cy5.5 fluorescence stability of the MTX-PEG-CS-IONPs-Cy5.5 in H_2O, PBS, 0.9% NaCl, 10% plasma, RPMI 1640, and FBS. Data were presented as mean ± SD ($n = 3$).

respectively.[12,19] Detail analysis was as follow. After the functionalization of MTX-PEG (see Figure 1B,C) on the surface of the CS-IONPs, an apparent increase of intensity at 2877 cm^{-1} was observed due to the alkyl C−H stretching vibration of PEG. The new peak at 1113 cm^{-1} was also present due to the C−O−C stretching vibration of PEG. The new peak at 1714 cm^{-1} was observed because of the new formation of the C═O stretching vibration originated from MTX. Moreover, the emergence of the new peaks at 1558 and 1650 cm^{-1} was suggestive of the generation of a new conjugate system. Combined with the above results of NMR and UV−vis analysis and the following results of change of particle size and zeta potential (discussed below), the FTIR result indicated the existence of the MTX-PEG-CS conjugate structure on the surface of the CS-IONPs.[6,19]

Table 1 also showed a comparison of the hydrodynamic particle size, PDI (an indicator of aggregation in the particles. As the value is higher, it shows a polydisperse system. As the value is lower and closer to zero, it denotes a monodisperse system), and zeta potential of CS-IONPs, PEG-CS-IONPs, and MTX-PEG-CS-IONPs. Surface functionalization with biomacromolecular drug was accompanied by both the hydrodynamic particle size and zeta potential changes of different formulations. After the modification of MTX-PEG, the hydrodynamic particle size become larger from 40.2 to 51.6 nm, and the zeta potential become smaller from 20.5 to 10.6 mV. The results were explained by the presence of MTX-PEG, which not only provided a steric

Table 1. R_2 Relaxivity, Hydrodynamic Particle Size, Polydispersity Index (PDI), and Zeta Potential of the CS-IONPs, PEG-CS-IONPs, and MTX-PEG-CS-IONPs in Water Determined by DLS. Data were Presented as Mean ± SD (n = 3)

	R_2 (mM^{-1} s^{-1})	hydrodynamic particle size (nm)	PDI	zeta potential (mV)
CS-IONPs	65.9 ± 0.7	40.2 ± 4.4	0.224 ± 0.017	20.5 ± 1.5
PEG-CS-IONPs	63.4 ± 0.9	42.6 ± 2.9	0.127 ± 0.010	11.7 ± 1.4
MTX-PEG-CS-IONPs	62.1 ± 1.4	51.6 ± 2.5	0.151 ± 0.013	10.6 ± 1.8

DOI: 10.1021/acsami.5b01685
ACS Appl. Mater. Interfaces 2015, 7, 11908−11920

barrier but also offered a charged barrier. Consistent with the above NMR, UV−vis, and FTIR results, the results were suggestive of the successful fabrication of the MTX-PEG-CS-IONPs. It was worth noting that the hydrodynamic particle size of the MTX-PEG-CS-IONPs determined by DLS after surface functionalization increased to some extent because of the presence of hydrated-layer formation, long PEG chains,[42] and MTX molecules. A particle size of the NPs around 200 nm was suited for the EPR effect, which was a prerequisite of the passive targeting.[43,44] An electrostatic repulsion force between the NPs with the same type of surface charge avoided the NPs aggregation and confer the NPs stability.[36,45] A specific superparamagnetic property with a high saturation magnetization value was sufficient for in vivo magnetic resonance imaging.[41] An excitation/emission in the NIR region was suitable for in vivo fluorescence imaging.[44] These results exhibited a prospect of the efficient and effective MTX-PEG-CS-IONPs-Cy5.5 with a nanoscaled particle size with a narrow particle size distribution (Figure 1E), a nonzero surface charge (Figure 1F), a near-spherical shape (Figure 1G), an approximate drug-loading content (6.27 ± 0.21%), a superparamagnetic behavior with a saturation magnetization of 36.5 emu/g (Figure 1H), a NIR emission (Figure 1I), and a well physiological stability (Figure 3B−D, discussed as below) for imaging, diagnosis, drug delivery, and cancer therapy.[1,6]

3.4. In Vitro Physiological Stability. The particle size of the MTX-PEG-CS-IONPs-Cy5.5 for biomedical applications should be small, uniform, and stable. A stability assay of particle size of the CS-IONPs-Cy5.5, PEG-CS-IONPs-Cy5.5, and MTX-PEG-CS-IONPs-Cy5.5 was performed under ultrapure water for 24 h. No obvious particle size change determined by DLS was exhibited in the PEG-CS-IONPs and MTX-PEG-CS-IONPs (Figure 3B). However, the CS-IONPs could show obvious aggregation and exhibit phase separation over 24 h in ultrapure water. It is now well-accepted that the surface of NPs would be covered by various types of proteins upon their entrance into the biological medium.[46] To further investigate the physiological stability of the PEG-CS-IONPs-Cy5.5 and MTX-PEG-CS-IONPs-Cy5.5 in biological medium, a particle size stability assay of the PEG-CS-IONPs-Cy5.5 and MTX-PEG-CS-IONPs-Cy5.5 was evaluated under six different biological media including ultrapure water, PBS, 0.9% (w/v) NaCl, 10% (v/v) plasma/heparin, RPMI 1640, and FBS for 24 h.[47] The MTX-PEG-CS-IONPs-Cy5.5 exhibited excellent stability (PEG-CS-IONPs-Cy5.5 showed a similar behavior, data not shown) in different biological mediums including the physiological environment of blood and cell at 37 °C (Figure 3C). Although the MTX-PEG-CS-IONPs-Cy5.5 showed the positive surface charge and might react with plasma protein with negative charge in the blood circulation, the presence of the high-density PEG brush layer as well as the structure integrity of the drug delivery systems could sufficiently preserve the physiological stability of the PEG-CS-IONPs-Cy5.5 and MTX-PEG-CS-IONPs-Cy5.5 against high ionic strength and nonspecific proteins adsorption under the physiological conditions.[36] In addition, the Cy5.5 fluorescence intensity of the PEG-CS-IONPs-Cy5.5 and MTX-PEG-CS-IONPs-Cy5.5 in different biological mediums did not also significantly change for 24 h, and their residual Cy5.5 fluorescence intensity remained at above 98% (Figure 3D, PEG-CS-IONPs-Cy5.5 showed a similar behavior, data not shown). Note that we chose the PEG-CS-IONPs-Cy5.5 instead of the CS-IONPs-Cy5.5 for comparison to MTX-PEG-CS-IONPs-Cy5.5 in the subsequent evaluations because of the limited physiological stability of the CS-IONPs-Cy5.5 (see Figure 3B).

3.5. In Vitro Drug Release. A variety of types of lysosomal proteases in tumor cells are capable of cleaving the amide linkage (also called peptide linkage),[48−50] which could release MTX in a free form into the cytoplasm of the cell to expose the anticancer activity. Thus, the in vitro MTX release behavior of the MTX-PEG-CS-IONPs-Cy5.5 as a function of time in PBS buffer solution with or without the presence of crude protease at different pH values were evaluated.

To simulate the bloodstream environment, the MTX-PEG-CS-IONPs-Cy5.5 were incubated with PBS at pH 7.4 without the presence of crude protease (Figure 4A). In striking contrast to

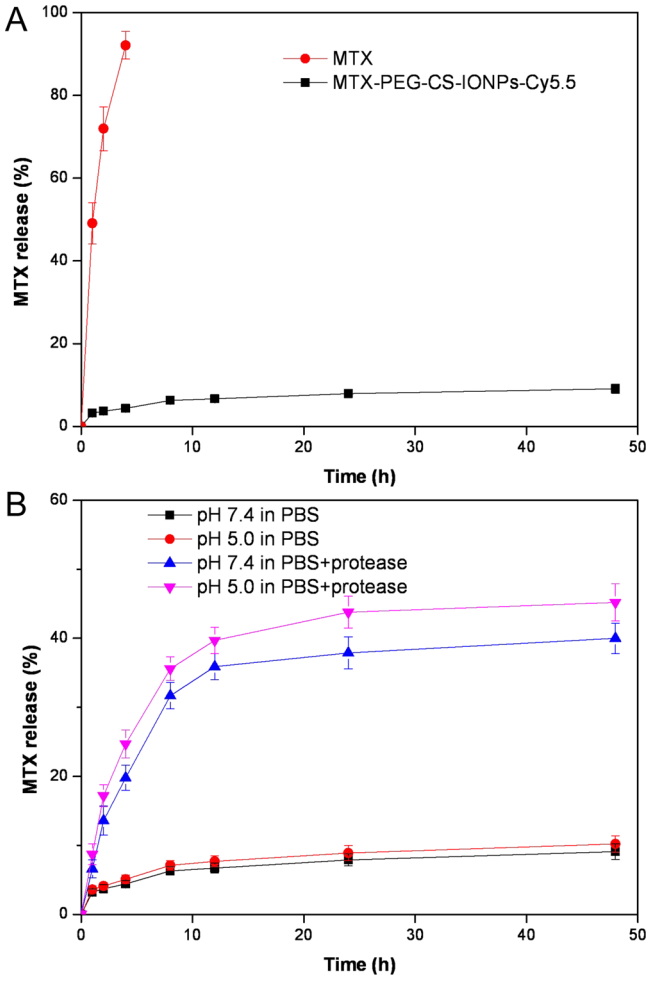

Figure 4. In vitro drug release profile of the MTX-PEG-CS-IONPs-Cy5.5. (A) Time-dependent drug release of MTX from the free MTX and the MTX-PEG-CS-IONPs-Cy5.5 in PBS without the presence of crude protease at pH 7.4 at 37 °C. Data were presented as mean ± SD (n = 3). (B) Time-dependent drug release of MTX from the MTX-PEG-CS-IONPs-Cy5.5 in PBS with or without the presence of crude protease at different pH values at 37 °C. Data were presented as mean ± SD (n = 3).

the free MTX with accumulative release amount of more than 90% over a short period of time (4 h), a much slower release of MTX from the MTX-PEG-CS-IONPs-Cy5.5 was clearly exhibited because of the delaying cleavage of amide linkages. However, at most 10% of drug from the MTX-PEG-CS-IONPs-Cy5.5 was released at pH 7.4 over 24 h.

DOI: 10.1021/acsami.5b01685
ACS Appl. Mater. Interfaces 2015, 7, 11908−11920

To simulate the tumor cellular acidic environment, the MTX-PEG-CS-IONPs-Cy5.5 were incubated with PBS at pH 5.0 with the presence of crude protease. As clearly shown in Figure 4B, the accumulative release amount of drug from MTX-PEG-CS-IONPs-Cy5.5 was highest at pH 5.0 with the presence of crude proteases over 48 h. The result indicated that the drug release was controlled by the dissociation of the drug from the NPs rather than by the simple diffusion of the drug from the NPs. More importantly, the pH sensitivity of the drug release rate with the presence of crude proteases was probably attributed to not only the pH effect on the cleavage of the amide bonds but also the additional pH effect on the protease activity. Although the activity of protease was stronger at lower pH, the activity of the protease would be declined with the extended time, and in turn the enzymatic cleavage was extremely slowed and therefore the release of the conjugated MTX from the NPs was almost completed within the first 12 h at pH 5.0.

The NPs with particle size around 200 nm was suited for systemic circulation and subsequent accumulation at the tumor site by the enhanced penetration and retention (EPR) effect,[43] which was a prerequisite of the passive targeting. Once intravenously administrated, the MTX-PEG-CS-IONPs-Cy5.5 could enable the minimum nonspecific drug release in the bloodstream (at off-target site), and hence greatly decrease the systemic toxicity. Once the MTX-PEG-CS-IONPs-Cy5.5 were accumulated in the tumor microenvironment by the EPR effect and then entered by tumor cells by FA receptor-mediated cellular uptale (at target site), the protease-dependent drug release as well as pH-dependent drug release could be significantly triggered due to the long-lasting activeness of intracellular proteases in the endo/lysosomes,[51] which offered an effective intracellular drug concentration for the enhanced therapeutic effects and the decreased side effects.

3.6. In Vitro Cellular Uptake. As is well-known, FA receptors are highly overexpressed on various cancer cells' surface and provide highly specific sites that differentiate cancer cells from normal cells. We selected FA receptor-overexpressed human cervical carcinoma HeLa cells[52,53] to investigate the cellular uptake of the PEG-CS-IONPs-Cy5.5 and MTX-PEG-CS-IONPs-Cy5.5 at the same Cy5.5 concentration using confocal laser scanning microscopy. To better compare the cell uptake between the PEG-CS-IONPs-Cy5.5 and MTX-PEG-CS-IONPs-Cy5.5, the images of cells were obtained under identical instrumental conditions. As shown in Figure 5A, the red fluorescence was observed within HeLa cells treated with the PEG-CS-IONPs-Cy5.5 and MTX-PEG-CS-IONPs-Cy5.5. More notably, the MTX modification improved the cellular uptake of the MTX-PEG-CS-IONPs-Cy5.5 in HeLa cells compared with the PEG-CS-IONPs-Cy5.5 after the same treatment time under the identical instrumental conditions. The result might be due to their different cellular uptake mechanisms. To assess the selectivity of the cellular uptake of the MTX-PEG-CS-IONPs-Cy5.5 in HeLa cells, the FA competition experiment was performed. The cellular uptake of the MTX-PEG-CS-IONPs-Cy5.5 by HeLa cells treated with excess of the free FA was drastically blocked compared with the untreated HeLa cells. In addition, the MTX modification did not significantly change the cellular uptake of the MTX-PEG-CS-IONPs-Cy5.5 in MC3T3-E1 cells (normal murine osteoblastic cells, normal cells) compared with the PEG-CS-IONPs-Cy5.5 (see Figure 6). All of the results indicated that the MTX-decorated PEG-CS-IONPs-Cy5.5 were able to specifically and selectively bind to cancer cells overexpressing FA repceptor.

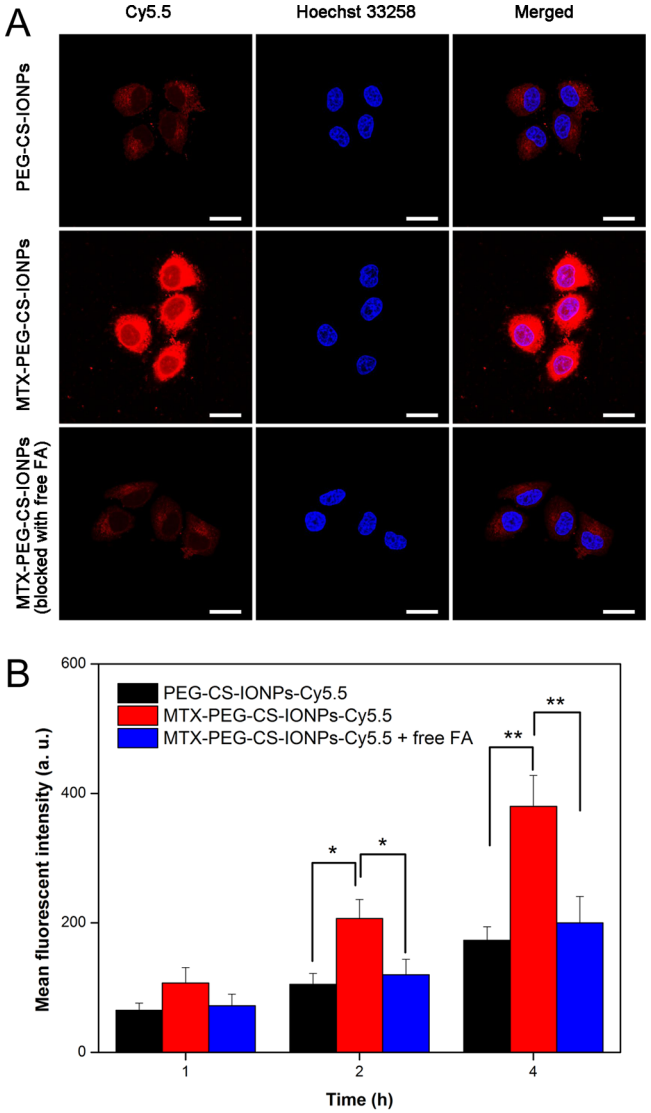

Figure 5. In vitro cellular uptake of the MTX-PEG-CS-IONPs-Cy5.5 in cancer cells. (A) Confocal laser scanning microscopy images of HeLa cells incubated with the PEG-CS-IONPs-Cy5.5, MTX-PEG-CS-IONPs-Cy5.5, and MTX-PEG-CS-IONPs-Cy5.5 under the free FA blocking. All the concentration of Cy5.5 was equivalent. All the scale bars represented 25 μm. All the images were taken under identical instrumental conditions (parameters such as laser power, offset, sensitivity, and gain constant were harmonized during the cell imaging procedure). (B) Flow cytometer tests of HeLa cells incubated with the PEG-CS-IONPs-Cy5.5 and MTX-PEG-CS-IONPs-Cy5.5, and MTX-PEG-CS-IONPs-Cy5.5 under the free FA blocking at the equivalent Cy5.5 concentration for 1, 2, and 4 h. Data were presented as mean ± SD (n = 3). * P < 0.05 (two-tailed).

3.7. Flow Cytometry. We next used flow cytometry to determine the quantitative cellular uptake of the PEG-CS-IONPs-Cy5.5 and MTX-PEG-CS-IONPs-Cy5.5 by HeLa cells. The mean fluorescence intensity of HeLa cells after 1, 2, and 4 h of incubation with the PEG-CS-IONPs-Cy5.5 and MTX-PEG-CS-IONPs-Cy5.5 were measured and shown in Figure 5B. The mean fluorescence intensity was straightly related to the mean number of the NPs uptaken by per cell. The mean fluorescence intensity of HeLa cells treated with the MTX-PEG-CS-IONPs-Cy5.5 was significantly higher than that of HeLa cells treated with the PEG-CS-IONPs-Cy5.5, further indicating the enhanced

DOI: 10.1021/acsami.5b01685
ACS Appl. Mater. Interfaces 2015, 7, 11908−11920

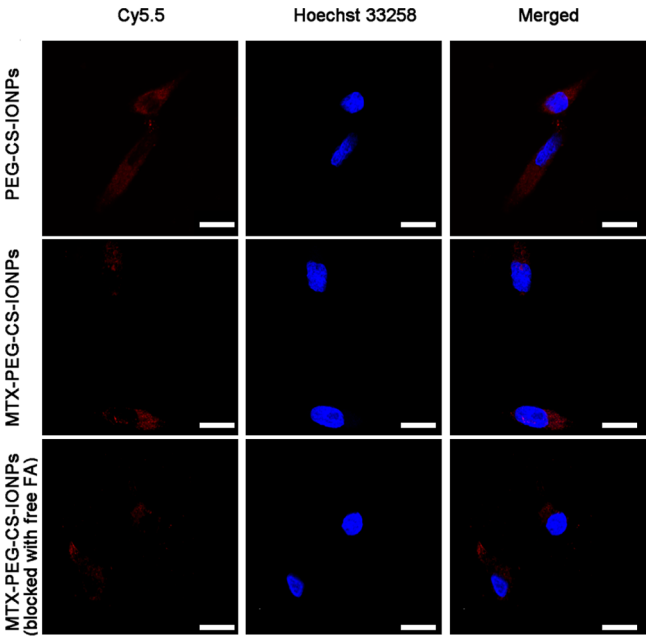

Figure 6. In vitro cellular uptake of the MTX-PEG-CS-IONPs-Cy5.5 in normal cells. Confocal laser scanning microscopy images of MC3T3-E1 cells incubated with the PEG-CS-IONPs-Cy5.5, MTX-PEG-CS-IONPs-Cy5.5, and MTX-PEG-CS-IONPs-Cy5.5 under the free FA blocking. All the concentration of Cy5.5 was equivalent. All the scale bars represented 25 μm. All the images were taken under identical instrumental conditions (parameters such as laser power, offset, sensitivity, and gain constant were harmonized during the cell imaging procedure).

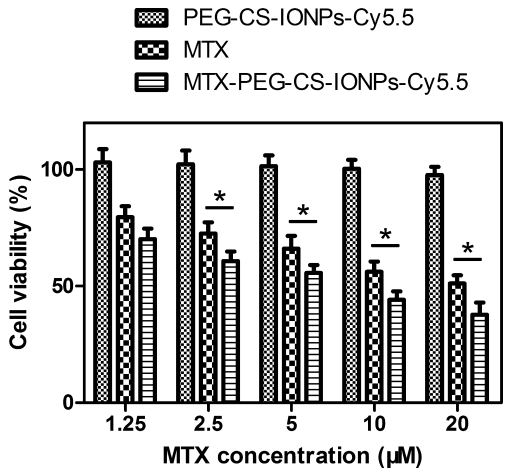

Figure 7. In vitro cell viability of the MTX-PEG-CS-IONPs-Cy5.5. Concentration-dependent cell viability of HeLa cells treated with the free MTX, PEG-CS-IONPs-Cy5.5, and MTX-PEG-CS-IONPs-Cy5.5 after incubation of 24 h. Data were presented as mean ± SD ($n = 6$). * $P < 0.05$ (two-tailed Student's t test).

cellular internalization of the MTX-PEG-CS-IONPs-Cy5.5 compared with the PEG-CS-IONPs-Cy5.5. The electrostatic interaction of the positive PEG-CS-IONPs-Cy5.5 (see Figure 1F) and the negative cell membrane of HeLa cell perhaps increased the cellular internalization of the PEG-CS-IONPs-Cy5.5. Furthermore, the selective interaction of the MTX functionalized PEG-CS-IONPs-Cy5.5 and the FA receptor overexpressed on HeLa cells' surface greatly increased the cellular internalization of MTX-PEG-CS-IONPs-Cy5.5. More notably, the mean fluorescence intensity of HeLa cells incubated the MTX-PEG-CS-IONPs-Cy5.5 under the free FA blocking was much lower than that of HeLa cells incubated with the PEG-CS-IONPs-Cy5.5 (Figure 5B). The result proved that the MTX-PEG-CS-IONPs-Cy5.5 entered the cancer cells through the FA receptor-mediated cellular uptake. These qualitative and quantitative results strongly supported the idea of the high targeting efficacy of the MTX-PEG-CS-IONPs-Cy5.5 to FA receptor-overexpressed cancer cells.

3.8. In Vitro Cell Viability. The in vitro cell viability of cancer cells treated with the MTX-PEG-CS-IONPs-Cy5.5 reflects their efficacy to kill cancer cells. The MTX-PEG-CS-IONPs-Cy5.5 and free MTX exhibited a concentration-dependent cytotoxicity on HeLa cells for 48 h (Figure 7). It was straightforward to explain that the greater cytotoxicity corresponded to the higher drug level. At the equivalent drug level, it was noted that the MTX-PEG-CS-IONPs-Cy5.5 significantly reduced the cell viability than the free MTX in the face of the fact that this cell line might be not resistant to MTX. No cytotoxicity of the MTX-free NPs (PEG-CS-IONPs-Cy5.5) was observed within the tested range of concentrations because of the biocompatibility of PEG and CS,[19] indicating that the PEG-CS-IONPs-Cy5.5 did not influence the action mechanism of MTX.

It should be pointed out that the observed cytotoxicity of the MTX-PEG-CS-IONPs-Cy5.5 was only due to MTX (the MTX-free NPs was noncytotoxicity). Therefore, these results were attributed to the highly selective targeting efficacy (FA receptor-mediated endocytosis, Figure 5) and efficiently controlled drug release (protease-dependent release as well as pH-dependent release, Figure 4) of the MTX-PEG-CS-IONPs-Cy5.5, which would efficiently improve the cellular uptake, accumulation, and retention of drug, increase the intracellular drug concentration, and hence enhance the cytotoxic activity. In a word, MTX with a dual function would be intracellularly released from the MTX-PEG-CS-IONPs-Cy5.5 in the tumor cells to "turn off" the targeting function of MTX and "turn on" the anticancer function of MTX for effective and efficient intracellular drug delivery.

3.9. In Vivo Pharmacokinetics. Since the characteristic of total body clearance of drugs in SD rats were comparable to that in humans, SD rats have been widely used as the animal model in the in vivo pharmacokinetics study.[54] To evaluate the pharmacokinetic profiles of the MTX-PEG-CS-IONPs-Cy5.5 in vivo, we treated SD rats with a single intravenous injection of the MTX-PEG-CS-IONPs-Cy5.5, collected plasma at different time intervals, and then determined the plasma concentration of MTX. The plasma concentration−time curve of MTX after systemic administration of the MTX-PEG-CS-IONPs-Cy5.5 and free MTX is shown in Figure 8. Plasma MTX concentration achieved the highest at the completion of in vivo systemic administration and progressively decreased as the time elapsed. It was found that the blood circulation time of the MTX-PEG-CS-IONPs-Cy5.5 was much prolonged over the free MTX, with significantly longer elimination half-life ($t_{1/2}$), higher area under the plasma concentration versus the time curve (AUC), longer mean residence time (MRT), and lower total body clearance (CL) in the blood clearance curves (Figure 8) and the pharmacokinetic parameters (Table 2). In agreement with other reports,[55] the slower clearance profile of the MTX-PEG-CS-IONPs-Cy5.5 compared with the free MTX indicated that both MTX- and PEG-decorated nanoscaled drug delivery systems was capable to reduce the undesired plasma protein adsorption (see Figure 3B) and the premature drug release in the

DOI: 10.1021/acsami.5b01685
ACS Appl. Mater. Interfaces 2015, 7, 11908−11920

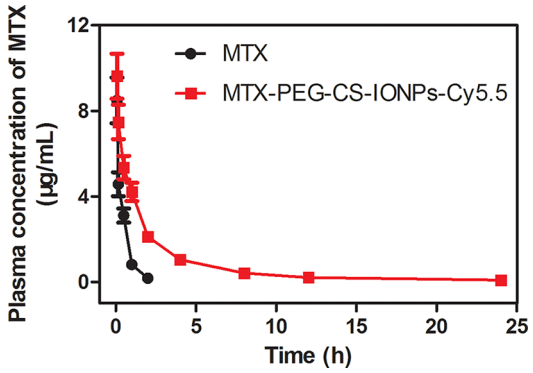

Figure 8. In vivo pharmacokinetic profile of the MTX-PEG-CS-IONPs-Cy5.5. Rats were intravenously injection with the free MTX and MTX-PEG-CS-IONPs-Cy5.5. Data were presented as mean ± SD (n = 6).

Table 2. Pharmacokinetic Parameters of MTX in Rats after Intravenous Administration of the Free MTX and MTX-PEG-CS-IONPs-Cy5.5

	MTX[a]	MTX-PEG-CS-IONPs-Cy5.5[a]
$t_{1/2}$ (h)	0.36 ± 0.07	3.57 ± 0.36[b]
$AUC_{0\text{-}t}$ (mg h L^{-1})	4.31 ± 0.31	18.32 ± 1.18[b]
$AUC_{0\text{-}\infty}$ (mg h L^{-1})	4.40 ± 0.33	18.85 ± 1.27[b]
$MRT_{0\text{-}t}$ (h)	0.38 ± 0.08	3.78 ± 0.45[b]
$MRT_{0\text{-}\infty}$ (h)	0.43 ± 0.11	4.40 ± 0.51[b]
CL (L h^{-1})	0.91 ± 0.04	0.21 ± 0.01[b]

[a]Data were presented as mean ± SD (n = 6). [b]$P < 0.05$ vs MTX.

bloodstream (see Figure 4A), increasing the blood persistence in the circulation and thus promoting the tumor accumulation by the enhanced penetration and retention (EPR) effect.

3.10. In Vivo Fluorescence Imaging. To investigate the potential of the MTX-PEG-CS-IONPs-Cy5.5 in vivo, the mice bearing HeLa tumor were intravenously administrated with the MTX-PEG-CS-IONPs-Cy5.5 via lateral tail vein. Figure 9A showed the in vivo real-time fluorescence imaging of the MTX-PEG-CS-IONPs-Cy5.5 in the HeLa tumor-bearing nude mice. The MTX-PEG-CS-IONPs-Cy5.5 were distributed in the body, then the Cy5.5 fluorescence signals became weaker. Within 12 h postinjection, the Cy5.5 fluorescence signals at the tumor site of the MTX-PEG-CS-IONPs-Cy5.5-treated mice were notably higher compared with the PEG-CS-IONPs-Cy5.5-treated mice (Figure 9A). The mice treated with the MTX-PEG-CS-IONPs-Cy5.5 were immediately euthanized at 12 h postinjection; subsequently, the tumor tissues as well as the normal tissues were isolated for ex vivo imaging and analysis. The fluorescence intensity in the tumor tissue of the MTX-PEG-CS-IONPs-Cy5.5-treated mice was significantly higher than that of the PEG-CS-IONPs-Cy5.5-treated mice (Figure 9B,C). In addition, the fluorescence intensity in the normal tissues, such as liver and lung of the MTX-PEG-CS-IONPs-Cy5.5-treated mice, was significantly lower than that of the PEG-CS-IONPs-Cy5.5-treated mice. Quantification of fluorescence signal intensities in the tissues stated that the tumor-targeting property of MTX could enrich the drug-delivery systems in the tumor as well as decrease their uptake in the liver, which was also confirmed by the bioquantification of Fe levels in the tissues (discussed below, see Figure 9F).[15] This result demonstrated that the MTX-PEG-CS-IONPs-Cy5.5 were preferentially accumulated at the site of tumor not only by the passive targeting (the particle size-mediated EPR effect as well as the PEG-mediated long-

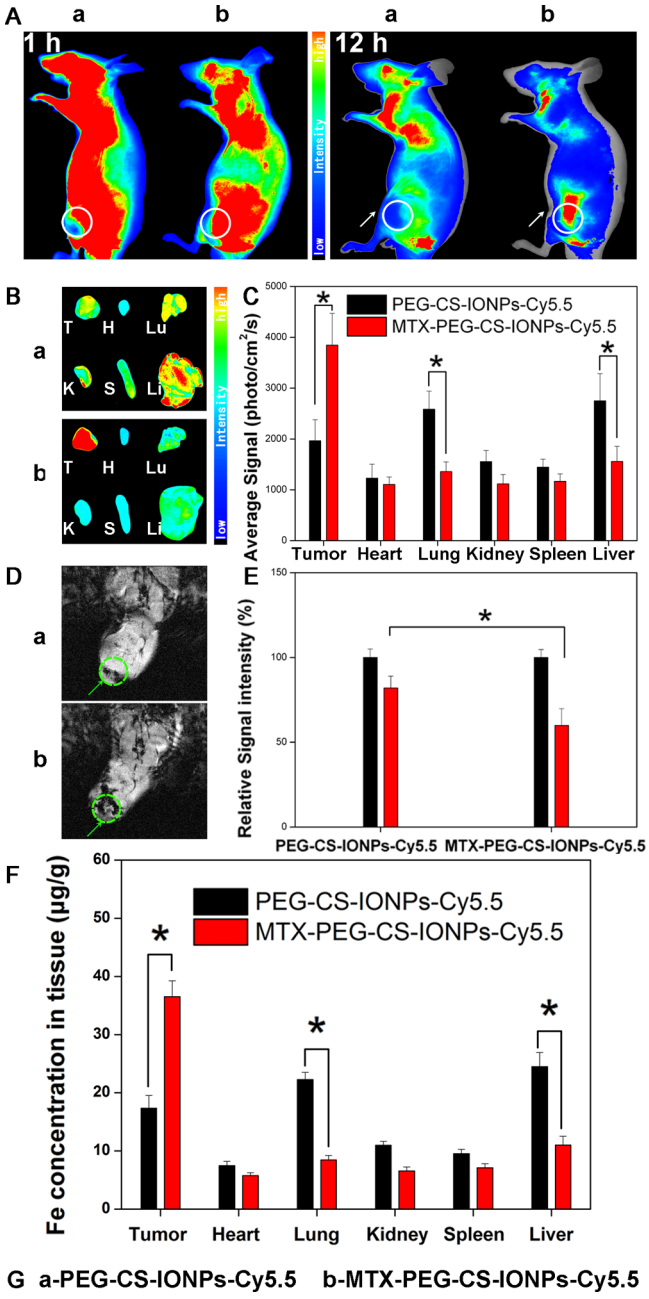

Figure 9. In vivo fluorescence imaging and magnetic resonance imaging of the MTX-PEG-CS-IONPs-Cy5.5. (A) In vivo fluorescence imaging of HeLa tumor-bearing mice after intravenous injection of the (a) PEG-CS-IONPs-Cy5.5 and (b) MTX-PEG-CS-IONPs-Cy5.5 at 12 h postinjection. Arrows indicated the sites of tumors. (B) Ex vivo fluorescence imaging of HeLa tumor-bearing mice after intravenous injection of the (a) PEG-CS-IONPs-Cy5.5 and (b) MTX-PEG-CS-IONPs-Cy5.5 at 12 h postinjection (T, tumor; H, heart; Lu, lung; K, kidney; S, spleen; Li, liver). (C) Average fluorescence signal intensities of tumors and normal tissues harvested from the HeLa tumor-bearing mice at 12 h post injection. Data were presented as mean ± SD (n = 3).* $P < 0.05$ (two-tailed Student's t test). (D) In vivo T2-weighted magnetic resonance images of tumor of mice after intravenous administration of the (a) PEG-CS-IONPs-Cy5.5 and (b) MTX-PEG-CS-IONPs-Cy5.5 at 12 h post injection. (E) Quantitative analysis results of signal intensities of tumors in the T2-weighted magnetic resonance images. Data were presented as mean ± SD (n = 3).* $P < 0.05$ (two-tailed Student's t-test). (F) Distribution profiles of Fe element in tumors and normal tissues at 12 h post injection.

DOI: 10.1021/acsami.5b01685
ACS Appl. Mater. Interfaces 2015, 7, 11908−11920

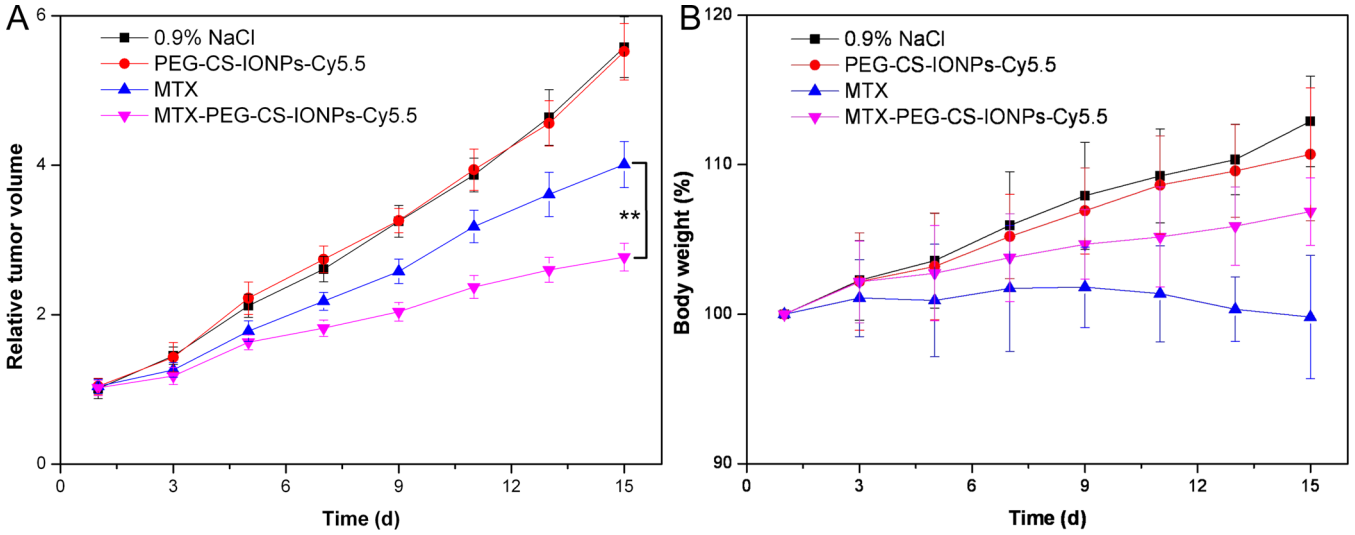

Figure 10. In vivo anticancer effect of the MTX-PEG-CS-IONPs-Cy5.5. (A) Tumor growth curves of HeLa tumor-bearing mice after intravenous injection of 0.9% NaCl, PEG-CS-IONPs-Cy5.5, free MTX, and MTX-PEG-CS-IONPs-Cy5.5. Data were presented as mean ± SD ($n = 6$).** $P < 0.01$ (two-tailed Student's t test). (B) Body weight variations of HeLa tumor-bearing mice after intravenous injection of 0.9% NaCl, PEG-CS-IONPs-Cy5.5, free MTX, and MTX-PEG-CS-IONPs-Cy5.5.

circulating effect) but also via the active targeting (the FA receptor-mediated endocytosis). These results also suggested that the utmost importance of the MTX functionalization offered the biocompatible, multifunctional, and therapeutic NPs a high tumor targeting efficacy.

3.11. In Vivo Magnetic Resonance Imaging. In vivo magnetic resonance imaging was evaluated using the same mice intravenously injected with the MTX-PEG-CS-IONPs-Cy5.5 for in vivo fluorescence imaging. T_2-weighted magnetic resonance images were obtained before and after the PEG-CS-IONPs-Cy5.5 and MTX-PEG-CS-IONPs-Cy5.5 injection. As shown in Figure 9D,E a significantly more decline in the magnetic resonance signal was exhibited in the tumor of the MTX-PEG-CS-IONPs-Cy5.5-treated mice compared with that of the PEG-CS-IONPs-Cy5.5-treated mice at 12 h after intravenous injection, indicating the greater tumor accumulation of the MTX-PEG-CS-IONPs-Cy5.5 over the PEG-CS-IONPs-Cy5.5. Quantifications of both Cy5.5 (see Figure 8C) and Fe levels (determined by inductively coupled plasma measurement) in the tissues (Figure 9F) also confirm the MTX-induced tumor targeting. In agreement with the above fluorescence imaging study and other reports,[38,56] the result demonstrated that the targeting ligand MTX facilitated the delivery of the MTX-PEG-CS-IONPs-Cy5.5 into FA receptor overexpressed tumor cells, thus rendering the MTX-PEG-CS-IONPs-Cy5.5 superior than the PEG-CS-IONPs-Cy5.5 delivered only through the EPR effect. Both results of the in vivo fluorescence imaging and magnetic resonance imaging also verified that the MTX-PEG-CS-IONPs-Cy5.5 could serve as a promising dual-modal probe for the simultaneous in vivo fluorescence and magnetic resonance imaging of FA receptor overexpressed tumor, which would offer more extensive imaging information and higher diagnostic precision.

3.12. In Vivo Anticancer Effect. Inspired by the high accumulation of MTX-PEG-CS-IONPs-Cy5.5 at the tumor site and their in vitro self-assisted anticancer activity, we further investigated the in vivo anticancer effect by using the HeLa tumor-bearing BALB/C mice. When tumors were increased to ~50−100 mm^3 in volume size (volume), the mice were randomly divided into five groups, and each group involved six mice. They were treated as follows: group 1, intravenous injection of 0.9% NaCl; group 2, intravenous injection of the free MTX injection; group 3, intravenous injection of the PEG-CS-IONPs-Cy5.5; group 4, intravenous injection of the MTX-PEG-CS-IONPs-Cy5.5. Tumor growth was clearly inhibited after the mice was intravenously injected with the free MTX and MTX-PEG-CS-IONPs-Cy5.5, compared with 0.9% NaCl and the PEG-CS-IONPs-Cy5.5 as a negative and positive control, respectively (Figure 10A). The result demonstrated that the inhibition effect of tumor growth after the mice were treated with the MTX-PEG-CS-IONPs-Cy5.5 was a result of the MTX-PEG-CS-IONPs-Cy5.5 mediated MTX delivery. Furthermore, the MTX-PEG-CS-IONPs-Cy5.5 group had significantly better anticancer efficacy than the free MTX group, due to their preferred tumor accumulation via the enhanced penetration and retention (EPR) effect and FA receptor-mediated endocytosis. In addition, the potential in vivo toxicity of NPs has usually been one of major concerns in the development of nanomedicines.[1,11] Thus, the body weight change of mice was determined to assess the in vivo toxicity. As shown in Figure 10B, the loss of body weight in mice was not found in the treatment with the MTX-PEG-CS-IONPs-Cy5.5, indicating a negligibly acute toxicity of the MTX-PEG-CS-IONPs-Cy5.5 at this dose. All of these results suggested that the longer circulation time (see Figure 8 and Table 2), the greater tumor accumulation (see Figure 9), the greater specific cellular uptake (see Figure 5 and 6), the more efficient controlled drug release (see Figure 4), and the stronger cytotoxicity (see Figure 7) of the MTX-PEG-CS-IONPs-Cy5.5 could lead to the high intracellular drug concentration of target cell, resulting in a significantly improved therapeutic efficacy with reduced toxicity of chemotherapy drug compared with the free MTX injection for clinical treatment.

4. CONCLUSIONS

In summary, we developed the biocompatible, multifunctional, and therapeutic NPs by the functionalization of MTX-PEG and Cy5.5 on the surface of the composite CS-IONPs. The versatile MTX-PEG-CS-IONPs-Cy5.5 had great potential in fluorescence

DOI: 10.1021/acsami.5b01685
ACS Appl. Mater. Interfaces 2015, 7, 11908−11920

and magnetic resonance imaging as self-targeted therapeutic drug delivery due to their superparamagnetic, fluorescent, targeting, and anticancer characters. Furthermore, the systemically administrated MTX-PEG-CS-IONPs-Cy5.5 efficiently resulted in higher tumor accumulation, more cell internalization, controlled drug release, improved therapeutic efficiency, and reduced side effects compared with the PEG-CS-IONPs-Cy5.5 and free MTX injection in vitro and in vivo. We anticipated that these multifunctional MTX-PEG-CS-IONPs-Cy5 would open numerous exciting opportunities in multimodal imaging, diagnosis, targeted drug delivery, and cancer therapy. Further studies of magnetic guidance and hyperthermia of the MTX-PEG-CS-IONPs-Cy5.5 are currently in progress.

AUTHOR INFORMATION

Corresponding Author

*E-mail: houzhenqing@xmu.edu.cn. Phone: +86-592-2189650. Fax: +86-592-2183058.

Notes

The authors declare no competing financial interest.

ACKNOWLEDGMENTS

This work was funded by the National Natural Science Foundation of China (Grant Nos. 31271071 and 81000660), the Fujian Province Medical Innovation Project (2014-CXB-350), the Army Logistics Scientific Research Project (CNJ14C007), and the Natural Science Foundation of Fujian Province of China (Grant No. 2013J01384).

REFERENCES

(1) Peer, D.; Karp, J. M.; Hong, S.; Farokhzad, O. C.; Margalit, R.; Langer, R. Nanocarriers as an Emerging Platform for Cancer Therapy. *Nat. Nanotechnol.* **2007**, *2*, 751−760.

(2) Jemal, A.; Bray, F.; Center, M. M.; Ferlay, J.; Ward, E.; Forman, D. Global Cancer Statistics. *Ca-Cancer J. Clin.* **2011**, *61*, 69−90.

(3) Lee, J. E.; Lee, N.; Kim, H.; Kim, J.; Choi, S. H.; Kim, J. H.; Kim, T.; Song, I. C.; Park, S. P.; Moon, W. K.; Hyeon, T. Uniform Mesoporous Dye-Doped Silica Nanoparticles Decorated with Multiple Magnetite Nanocrystals for Simultaneous Enhanced Magnetic Resonance Imaging, Fluorescence Imaging, and Drug Delivery. *J. Am. Chem. Soc.* **2010**, *132*, 552−557.

(4) Gao, J.; Gu, H.; Xu, B. Multifunctional Magnetic Nanoparticles: Design, Synthesis, and Biomedical Applications. *Acc. Chem. Res.* **2009**, *42*, 1097−1107.

(5) Yallapu, M. M.; Othman, S. F.; Curtis, E. T.; Gupta, B. K.; Jaggi, M.; Chauhan, S. C. Multi-Functional Magnetic Nanoparticles for Magnetic Resonance Imaging and Cancer Therapy. *Biomaterials* **2011**, *32*, 1890−1905.

(6) Yoo, M. K.; Park, I. K.; Lim, H. T.; Lee, S. J.; Jiang, H. L.; Kim, Y. K.; Choi, Y. J.; Cho, M. H.; Cho, C. S. Folate-Peg-Superparamagnetic Iron Oxide Nanoparticles for Lung Cancer Imaging. *Acta Biomater.* **2012**, *8*, 3005−3013.

(7) Fortin, J. P.; Wilhelm, C.; Servais, J.; Menager, C.; Bacri, J. C.; Gazeau, F. Size-Sorted Anionic Iron Oxide Nanomagnets as Colloidal Mediators for Magnetic Hyperthermia. *J. Am. Chem. Soc.* **2007**, *129*, 2628−2635.

(8) Gao, X.; Cui, Y.; Levenson, R. M.; Chung, L. W.; Nie, S. In Vivo Cancer Targeting and Imaging with Semiconductor Quantum Dots. *Nat. Biotechnol.* **2004**, *22*, 969−976.

(9) Michalet, X.; Pinaud, F. F.; Bentolila, L. A.; Tsay, J. M.; Doose, S.; Li, J. J.; Sundaresan, G.; Wu, A. M.; Gambhir, S. S.; Weiss, S. Quantum Dots for Live Cells, in Vivo Imaging, and Diagnostics. *Science* **2005**, *307*, 538−544.

(10) Jain, P. K.; Huang, X.; El-Sayed, I. H.; El-Sayed, M. A. Noble Metals on the Nanoscale: Optical and Photothermal Properties and Some Applications in Imaging, Sensing, Biology, and Medicine. *Acc. Chem. Res.* **2008**, *41*, 1578−1586.

(11) Farokhzad, O. C.; Langer, R. Impact of Nanotechnology on Drug Delivery. *ACS Nano* **2009**, *3*, 16−20.

(12) Arias, J. L.; Reddy, L. H.; Couvreur, P. Fe3o4/Chitosan Nanocomposite for Magnetic Drug Targeting to Cancer. *J. Mater. Chem.* **2012**, *22*, 7622−7632.

(13) Kong, S. D.; Sartor, M.; Hu, C. M.; Zhang, W.; Zhang, L.; Jin, S. Magnetic Field Activated Lipid-Polymer Hybrid Nanoparticles for Stimuli-Responsive Drug Release. *Acta Biomater.* **2013**, *9*, 5447−5452.

(14) Ma, Y.; Tong, S.; Bao, G.; Gao, C.; Dai, Z. Indocyanine Green Loaded Spio Nanoparticles with Phospholipid-Peg Coating for Dual-Modal Imaging and Photothermal Therapy. *Biomaterials* **2013**, *34*, 7706−7714.

(15) Tian, Y.; Jiang, X.; Chen, X.; Shao, Z.; Yang, W. Doxorubicin-Loaded Magnetic Silk Fibroin Nanoparticles for Targeted Therapy of Multidrug-Resistant Cancer. *Adv. Mater.* **2014**, *26*, 7393−7398.

(16) Lin, L. S.; Cong, Z. X.; Cao, J. B.; Ke, K. M.; Peng, Q. L.; Gao, J.; Yang, H. H.; Liu, G.; Chen, X. Multifunctional Fe(3)O(4)@Polydopamine Core-Shell Nanocomposites for Intracellular Mrna Detection and Imaging-Guided Photothermal Therapy. *ACS Nano* **2014**, *8*, 3876−3883.

(17) Huang, P.; Song, H.; Wang, W.; Sun, Y.; Zhou, J.; Wang, X.; Liu, J.; Liu, J.; Kong, D.; Dong, A. Integrin-Targeted Zwitterionic Polymeric Nanoparticles with Acid-Induced Disassembly Property for Enhanced Drug Accumulation and Release in Tumor. *Biomacromolecules* **2014**, *15*, 3128−3138.

(18) Zhou, S. F.; Li, Y.; Cui, F.; Jia, M. M.; Yang, X. R.; Wang, Y. G.; Xie, L. Y.; Zhang, Q. Q.; Hou, Z. Q. Development of Multifunctional Folate-Poly(Ethylene Glycol)-Chitosan-Coated Fe3o4 Nanoparticles for Biomedical Applications. *Macromol. Res.* **2014**, *22*, 58−66.

(19) Hou, Z.; Zhan, C.; Jiang, Q.; Hu, Q.; Li, L.; Chang, D.; Yang, X.; Wang, Y.; Li, Y.; Ye, S.; Xie, L.; Yi, Y.; Zhang, Q. Both Fa- and Mpeg-Conjugated Chitosan Nanoparticles for Targeted Cellular Uptake and Enhanced Tumor Tissue Distribution. *Nanoscale Res. Lett.* **2011**, *6*, 563.

(20) Jia, M.; Li, Y.; Yang, X.; Huang, Y.; Wu, H.; Huang, Y.; Lin, J.; Li, Y.; Hou, Z.; Zhang, Q. Development of Both Methotrexate and Mitomycin C Loaded Pegylated Chitosan Nanoparticles for Targeted Drug Codelivery and Synergistic Anticancer Effect. *ACS Appl. Mater. Interfaces* **2014**, *6*, 11413−11423.

(21) Jolivet, J.; Cowan, K. H.; Curt, G. A.; Clendeninn, N. J.; Chabner, B. A. The Pharmacology and Clinical Use of Methotrexate. *N. Engl. J. Med.* **1983**, *309*, 1094−1104.

(22) Chabner, B. A.; Roberts, T. G., Jr. Timeline: Chemotherapy and the War on Cancer. *Nat. Rev. Cancer* **2005**, *5*, 65−72.

(23) van Vlerken, L. E.; Vyas, T. K.; Amiji, M. M. Poly(Ethylene Glycol)-Modified Nanocarriers for Tumor-Targeted and Intracellular Delivery. *Pharm. Res.* **2007**, *24*, 1405−1414.

(24) Chen, C.; Ke, J.; Zhou, X. E.; Yi, W.; Brunzelle, J. S.; Li, J.; Yong, E. L.; Xu, H. E.; Melcher, K. Structural Basis for Molecular Recognition of Folic Acid by Folate Receptors. *Nature* **2013**, *500*, 486−489.

(25) Thomas, T. P.; Huang, B.; Choi, S. K.; Silpe, J. E.; Kotlyar, A.; Desai, A. M.; Zong, H.; Gam, J.; Joice, M.; Baker, J. R., Jr. Polyvalent Dendrimer-Methotrexate as a Folate Receptor-Targeted Cancer Therapeutic. *Mol. Pharmaceutics* **2012**, *9*, 2669−2676.

(26) Li, Y.; Lin, J.; Wu, H.; Jia, M.; Yuan, C.; Chang, Y.; Hou, Z.; Dai, L. Novel Methotrexate Prodrug-Targeted Drug Delivery System Based on Peg-Lipid-Pla Hybrid Nanoparticles for Enhanced Anticancer Efficacy and Reduced Toxicity of Mitomycin C. *J. Mater. Chem. B* **2014**, *2*, 6534−6548.

(27) Luo, F.; Li, Y.; Jia, M.; Cui, F.; Wu, H.; Yu, F.; Lin, J.; Yang, X.; Hou, Z.; Zhang, Q. Validation of a Janus Role of Methotrexate-Based Pegylated Chitosan Nanoparticles in Vitro. *Nanoscale Res. Lett.* **2014**, *9*, 363.

(28) Rijnboutt, S.; Jansen, G.; Posthuma, G.; Hynes, J. B.; Schornagel, J. H.; Strous, G. J. Endocytosis of Gpi-Linked Membrane Folate Receptor-Alpha. *J. Cell Biol.* **1996**, *132*, 35−47.

(29) Qiu, A.; Jansen, M.; Sakaris, A.; Min, S. H.; Chattopadhyay, S.; Tsai, E.; Sandoval, C.; Zhao, R.; Akabas, M. H.; Goldman, I. D.

DOI: 10.1021/acsami.5b01685
ACS Appl. Mater. Interfaces 2015, 7, 11908−11920

Identification of an Intestinal Folate Transporter and the Molecular Basis for Hereditary Folate Malabsorption. *Cell* **2006**, *127*, 917−928.
(30) Mizusawa, K.; Takaoka, Y.; Hamachi, I. Specific Cell Surface Protein Imaging by Extended Self-Assembling Fluorescent Turn-on Nanoprobes. *J. Am. Chem. Soc.* **2012**, *134*, 13386−13395.
(31) Rogachev, A. Y.; Hoffmann, R. Iodine (I2) as a Janus-Faced Ligand in Organometallics. *J. Am. Chem. Soc.* **2013**, *135*, 3262−3275.
(32) Dopieralski, P.; Ribas-Arino, J.; Anjukandi, P.; Krupicka, M.; Kiss, J.; Marx, D. The Janus-Faced Role of External Forces in Mechanochemical Disulfide Bond Cleavage. *Nat. Chem.* **2013**, *5*, 685−691.
(33) Wilson, S. B.; Delovitch, T. L. Janus-Like Role of Regulatory Inkt Cells in Autoimmune Disease and Tumour Immunity. *Nat. Rev. Immunol.* **2003**, *3*, 211−222.
(34) Laurent, S.; Forge, D.; Port, M.; Roch, A.; Robic, C.; Vander Elst, L.; Muller, R. N. Magnetic Iron Oxide Nanoparticles: Synthesis, Stabilization, Vectorization, Physicochemical Characterizations, and Biological Applications. *Chem. Rev.* **2008**, *108*, 2064−2110.
(35) Jager, E.; Jager, A.; Chytil, P.; Etrych, T.; Rihova, B.; Giacomelli, F. C.; Stepanek, P.; Ulbrich, K. Combination Chemotherapy Using Core-Shell Nanoparticles through the Self-Assembly of Hpma-Based Copolymers and Degradable Polyester. *J. Controlled Release* **2013**, *165*, 153−161.
(36) Li, Y.; Wu, H.; Yang, X.; Jia, M.; Li, Y.; Huang, Y.; Lin, J.; Wu, S.; Hou, Z. Mitomycin C-Soybean Phosphatidylcholine Complex-Loaded Self-Assembled Peg-Lipid-Pla Hybrid Nanoparticles for Targeted Drug Delivery and Dual-Controlled Drug Release. *Mol. Pharmaceutics* **2014**, *11*, 2915−2927.
(37) Lin, J.; Li, Y.; Wu, H.; Yang, X.; Li, Y.; Ye, S.; Hou, Z.; Lin, C. Tumor-Targeted Co-Delivery of Mitomycin C and 10-Hydroxycamptothecin Via Micellar Nanocarriers for Enhanced Anticancer Efficacy. *RSC Adv.* **2015**, *5*, 23022−23033.
(38) Niu, D.; Luo, X.; Li, Y.; Liu, X.; Wang, X.; Shi, J. Manganese-Loaded Dual-Mesoporous Silica Spheres for Efficient T1- and T2-Weighted Dual Mode Magnetic Resonance Imaging. *ACS Appl. Mater. Interfaces* **2013**, *5*, 9942−9948.
(39) Cao, D.; Tian, S.; Huang, H.; Chen, J.; Pan, S. Divalent Folate Modification on Peg: An Effective Strategy for Improving the Cellular Uptake and Targetability of Pegylated Polyamidoamine-Polyethylenimine Copolymer. *Mol. Pharmaceutics* **2015**, *12*, 240−252.
(40) Young, K. L.; Xu, C.; Xie, J.; Sun, S. Conjugating Methotrexate to Magnetite (Fe(3)O(4)) Nanoparticles Via Trichloro-S-Triazine. *J. Mater. Chem.* **2009**, *19*, 6400−6406.
(41) Li, K.; Ding, D.; Huo, D.; Pu, K.-Y.; Thao, N. N. P.; Hu, Y.; Li, Z.; Liu, B. Conjugated Polymer Based Nanoparticles as Dual-Modal Probes for Targeted in Vivo Fluorescence and Magnetic Resonance Imaging. *Adv. Funct. Mater.* **2012**, *22*, 3107−3115.
(42) Ni, D.; Zhang, J.; Bu, W.; Xing, H.; Han, F.; Xiao, Q.; Yao, Z.; Chen, F.; He, Q.; Liu, J.; Zhang, S.; Fan, W.; Zhou, L.; Peng, W.; Shi, J. Dual-Targeting Upconversion Nanoprobes across the Blood-Brain Barrier for Magnetic Resonance/Fluorescence Imaging of Intracranial Glioblastoma. *ACS Nano* **2014**, *8*, 1231−1242.
(43) Torchilin, V. Tumor Delivery of Macromolecular Drugs Based on the Epr Effect. *Adv. Drug Delivery Rev.* **2011**, *63*, 131−135.
(44) Li, Y.; Wu, H.; Jia, M.; Cui, F.; Lin, J.; Yang, X.; Wang, Y.; Dai, L.; Hou, Z. Therapeutic Effect of Folate-Targeted and Pegylated Phytosomes Loaded with a Mitomycin C-Soybean Phosphatidyhlcholine Complex. *Mol. Pharmaceutics* **2014**, *11*, 3017−3026.
(45) Petros, R. A.; DeSimone, J. M. Strategies in the Design of Nanoparticles for Therapeutic Applications. *Nat. Rev. Drug Discovery* **2010**, *9*, 615−627.
(46) Lundqvist, M.; Stigler, J.; Elia, G.; Lynch, I.; Cedervall, T.; Dawson, K. A. Nanoparticle Size and Surface Properties Determine the Protein Corona with Possible Implications for Biological Impacts. *Proc. Natl. Acad. Sci. U. S. A.* **2008**, *105*, 14265−14270.
(47) Zheng, M.; Zhao, P.; Luo, Z.; Gong, P.; Zheng, C.; Zhang, P.; Yue, C.; Gao, D.; Ma, Y.; Cai, L. Robust Icg Theranostic Nanoparticles for Folate Targeted Cancer Imaging and Highly Effective Photothermal Therapy. *ACS Appl. Mater. Interfaces* **2014**, *6*, 6709−6716.
(48) Poole, A. R.; Tiltman, K. J.; Recklies, A. D.; Stoker, T. A. M. Differences in Secretion of the Proteinase Cathepsin B at the Edges of Human Breast Carcinomas and Fibroadenomas. *Nature* **1978**, *273*, 545−547.
(49) Weissleder, R.; Tung, C. H.; Mahmood, U.; Bogdanov, A., Jr. In Vivo Imaging of Tumors with Protease-Activated near-Infrared Fluorescent Probes. *Nat. Biotechnol.* **1999**, *17*, 375−378.
(50) Li, Y.; Lin, J.; Wu, H.; Chang, Y.; Yuan, C.; Liu, C.; Wang, S.; Hou, Z.; Dai, L. Orthogonally Functionalized Nanoscale Micelles for Active Targeted Codelivery of Methotrexate and Mitomycin C with Synergistic Anticancer Effect. *Mol. Pharmaceutics* **2015**, *12*, 769−782.
(51) Moghimi, S. M.; Hunter, A. C.; Murray, J. C. Long-Circulating and Target-Specific Nanoparticles: Theory to Practice. *Pharmacol. Rev.* **2001**, *53*, 283−318.
(52) Lv, R.; Yang, P.; He, F.; Gai, S.; Li, C.; Dai, Y.; Yang, G.; Lin, J. A Yolk-Like Multifunctional Platform for Multimodal Imaging and Synergistic Therapy Triggered by a Single near-Infrared Light. *ACS Nano* **2015**, *9*, 1630−1647.
(53) Lv, R.; Yang, P.; He, F.; Gai, S.; Yang, G.; Lin, J. Hollow Structured Y2o3:Yb/Er−Cuxs Nanospheres with Controllable Size for Simultaneous Chemo/Photothermal Therapy and Bioimaging. *Chem. Mater.* **2015**, *27*, 483−496.
(54) Kim, S.; Choi, Y.; Lee, M. Pharmacokinetics and Pharmacodynamics of Furosemide in Protein-Calorie Malnutrition. *J. Pharmacokinet. Biopharm.* **1993**, *21*, 1−17.
(55) Li, M.; Song, W.; Tang, Z.; Lv, S.; Lin, L.; Sun, H.; Li, Q.; Yang, Y.; Hong, H.; Chen, X. Nanoscaled Poly(L-Glutamic Acid)/Doxorubicin-Amphiphile Complex as Ph-Responsive Drug Delivery System for Effective Treatment of Nonsmall Cell Lung Cancer. *ACS Appl. Mater. Interfaces* **2013**, *5*, 1781−1792.
(56) Chang, Y.; Liu, N.; Chen, L.; Meng, X.; Liu, Y.; Li, Y.; Wang, J. Synthesis and Characterization of Dox-Conjugated Dendrimer-Modified Magnetic Iron Oxide Conjugates for Magnetic Resonance Imaging, Targeting, and Drug Delivery. *J. Mater. Chem.* **2012**, *22*, 9594−9601.

DOI: 10.1021/acsami.5b01685
ACS Appl. Mater. Interfaces 2015, 7, 11908−11920